Observed Dispersion Relation of Yanai Waves and 17-Day Tropical Instability Waves in the Pacific Ocean

Toshiaki Shinoda
Naval Research Laboratory, Stennis Space Center, Mississippi, USA

Abstract

Using sea surface height (SSH) data derived from recent satellite observations, we present the observed dispersion relationship of mixed Rossby Gravity (Yanai) waves in the Pacific Ocean. A wavenumber-frequency spectral analysis of SSH fields shows prominent spectral peaks along the dispersion curves of first and second baroclinic mode oceanic Yanai waves. Also, salient features of tropical instability waves (TIWs) with a period of ~17 days can be effectively isolated based on a cross-correlation analysis of sea surface temperature (SST) and SSH time series that are filtered in wavenumber-frequency domain. These statistical representations of oceanic Yanai waves and TIWs are important for the evaluation of numerical model simulations of these waves and for improving our understanding of the physics of 17-day TIWs.

1. Introduction

Mixed Rossby-Gravity waves (often referred to as Yanai waves) play an important role in a variety of phenomena in the tropical ocean and atmosphere (e.g., Yanai and Hayashi 1969; Zangvil 1975; Liebmann and Hendon 1990; Takayabu and Nitta 1993; Lyman et al. 2007). The dispersion relation and the structure of Yanai waves were derived as one of the eigenmodes of a linearized shallow water equations on an equatorial β-plane (Matsuno 1966). Shortly after the derivation of the theoretical solution, observational evidence of Yanai waves was found by the analysis of winds in the lower stratosphere (Yanai and Maruyama 1966). Since then, many studies identified their generation and propagation, and discussed their characteristics and forcing mechanism in both the ocean and atmosphere (e.g., Wunsch and Gill 1976; Weisberg et al. 1979; Itoh and Ghil 1988; Zhu et al. 1998). A particular interest to the present study is the in-situ data analysis which shows the structure of tropical instability waves (TIWs) with a ~17-day period that is consistent with a surface trapped Yanai wave (Lyman et al. 2007).

Using outgoing longwave radiation (OLR) data, the observed dispersion relationship of atmospheric Yanai waves coupled to convection was described in frequency-wavenumber space (Wheeler and Kiladis 1999). It is demonstrated that wavenumber-frequency spectral analysis is useful for identifying signals of atmospheric equatorial waves including Yanai waves, and for isolating their structure. While the observed dispersion relationships of equatorial Kelvin and Rossby waves in the ocean were identified recently by wavenumber-frequency spectra of satellite-derived sea surface height (SSH) (Wakata 2007; Farrar 2008; Shinoda et al. 2009), the resolution of the satellite altimeter data was insufficient to describe oceanic Yanai waves in frequency-wavenumber space until recently. This situation has begun to change because of multiple satellite launches in recent years. Compared to previous altimeter data used to identify oceanic equatorial Kelvin and Rossby waves (TOPEX/Poseidon), the resolution of recent altimetry products has been substantially improved by using measurements from multi-satellites, and it is now feasible to resolve signals of oceanic Yanai waves for a wide range of frequency-wavenumber domains. In this study, we applied wavenumber-frequency spectral analysis to identify the observed dispersion relation of oceanic Yanai waves using high resolution SSH data measured by satellite altimetry. Also, further statistical analyses were performed to isolate TIWs with a ~17-day period (referred to as "17-day TIWs" hereafter), which have characteristics similar to Yanai waves.

Corresponding author: Toshiaki Shinoda, Naval Research Laboratory, Stennis Space Center, Mississippi, 39529, USA. E-mail: toshiaki.shinoda@nrlssc.navy.mil.

2. Wavenumber-frequency spectral analysis

Wavenumber-frequency spectral analysis was applied to identify oceanic Yanai waves using SSH and SST data. Daily average SSH anomalies derived from multi-satellite altimeters, which are distributed by Archiving, Validation and Interpretation of Satellite Oceanographic data (AVISO), are used to identify signals of Yanai waves and 17-day TIWs. Data for the 7-year period of 2002–2008 with the horizontal grid spacing of 1° are analyzed. The TRMM Microwave Imager (TMI) SST data for the same period (2002–2008) are also analyzed to describe the structure of 17-day TIWs. The 3-day average TMI SST data are originally gridded at 0.25° × 0.25°. We average the data onto a 1° × 1° grid for comparison with the analysis of SSH. It should be noted that the 1° × 1° gridded SSH data are a smoothed version of the measurements, which are derived by the objective analysis, and that the actual resolution of the data is still uncertain (e.g., Chelton and Schlax 2003).

Since the structure of Yanai wave is anti-symmetric about the equator, the anomalies of SSH and SST data are first decomposed to anti-symmetric and symmetric components (Wheeler and Kiladis 1999). Then a complex FFT of SSH anomalies is done over longitude to decompose SSH into zonal wavenumbers, and an additional FFT is used to determine the spectral power of each resolved wavenumber by frequency.

Figure 1a shows contours of the base 10 logarithm of power in wavenumber-frequency space calculated from anti-symmetric component of SSH anomalies in the equatorial area (5°N–5°S) in the Pacific Ocean (east of 160°E). Here, the background spectrum is removed from the original spectrum (Wheeler and Kiladis 1999; Shinoda et al. 2009). Prominent spectral signals of Yanai wave are evident, with their peak corresponding to the dispersion curve of an equivalent depth 0.8 m. This equivalent depth corresponds to equatorial Kelvin waves with a phase speed of ~2.8 m s^{-1}, consistent with the first baroclinic mode Kelvin waves in the equatorial Pacific Ocean (e.g., Cravatte et al. 2003; Shinoda et al. 2008). Signals of the second baroclinic mode Yanai wave are also found for the equivalent depth of 0.26 m (Kelvin wave phase speed of ~1.6 m s^{-1}), which are comparable to those for the first baroclinic mode.

Figure 1b shows the spectrum calculated from the same analysis using the TMI SST. While signals of Yanai waves for the wide range of the dispersion curve is not as clear as in the SSH data, broad peaks at around a period of ~17 days and wavelength ~1500 km are evident. These frequencies and wavenumbers are consistent with those associated with TIWs detected from in-situ observations (e.g., Halpern et al. 1988; Qiao and Weisberg 1995; Lyman et al. 2007). Also, the result is consistent with a previous study suggesting that 17-day TIWs have characteristics similar to an unstable Yanai wave (Lyman et al. 2007). However, the meridional structure of TIWs is not exactly the same as that of a Yanai wave derived from linear shallow water equations because of strong mean currents in this region. It should be noted that we have also calculated the spectrum using total (symmetric plus anti-symmetric components) SST anomalies for the area 5°N–0°, and that we found similar peaks around a period of ~17 days.

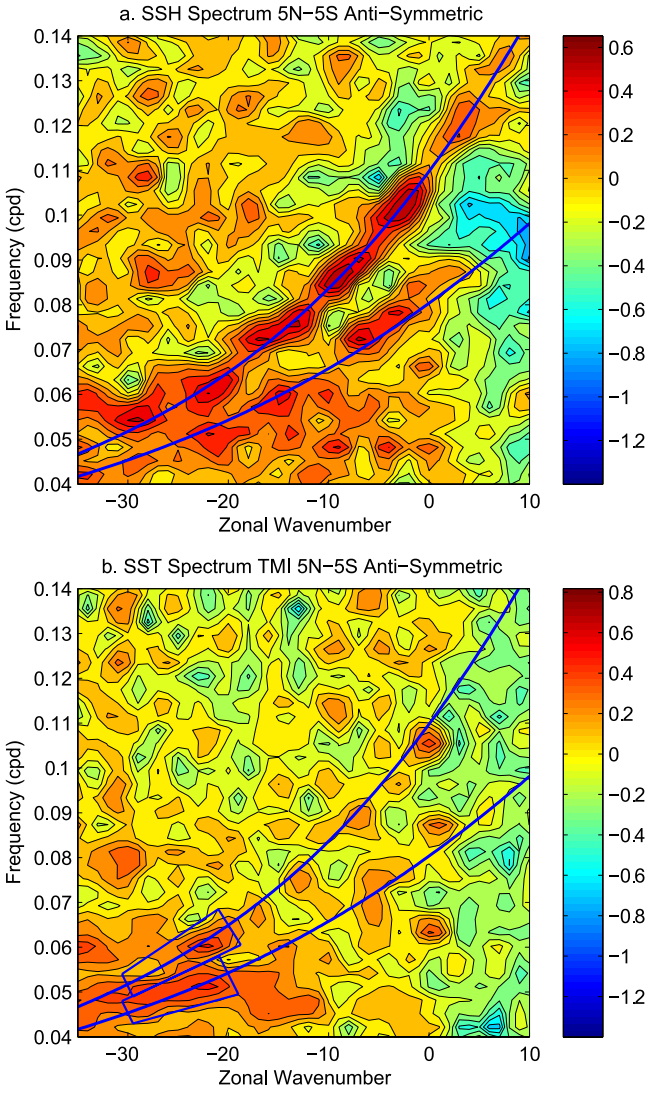

Fig. 1. (a) Zonal wavenumber-frequency power spectrum of SSH anomalies. The number of the color bar indicates the base-10 logarithm. The curves indicate Yanai wave dispersion relation for equivalent depths of 0.8 m and 0.26 m. (b) Same as (a) except for SST anomalies.

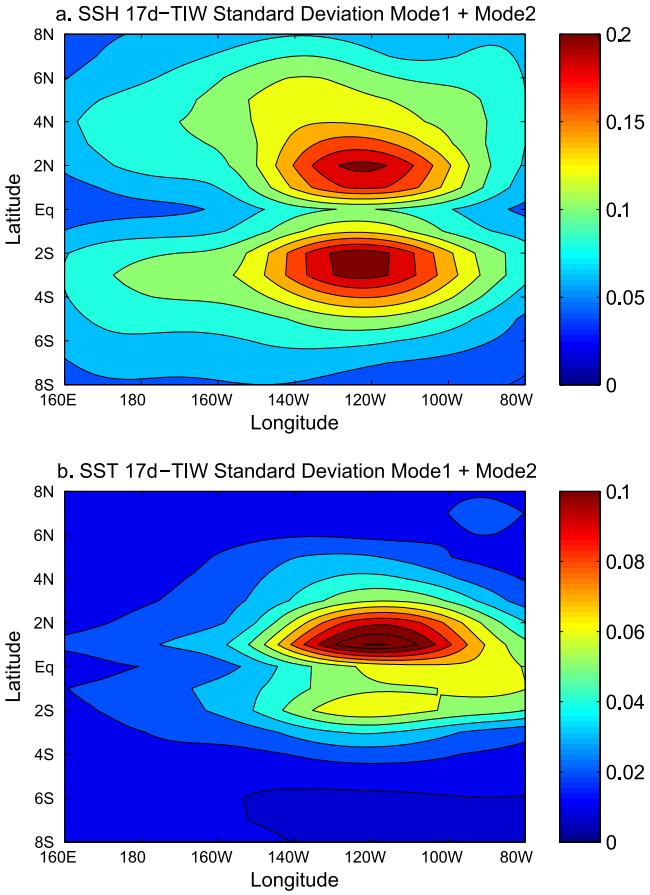

Fig. 2. (a) Standard deviation of SSH anomalies (cm) filtered at periods and wavelength in the area surrounded by the two boxes shown in Fig. 1b. (b) Same as (a) except for SST anomalies.

In order to describe the spatial variation of TIW activity, space and time filtering (via spectral transform) centered around the spectral peak (the area of two boxes in Fig. 1b) is applied to the time series of SSH and SST. Figure 2a shows the standard deviation of SSH time series at each location that are filtered in space and time for the area surrounded by two boxes in Fig. 1b. The area includes signals of both first and second baroclinic mode Yanai waves. In contrast to SSH signals of TIWs with a 33-day period in which the maximum is located around 5°N (e.g., Miller et al. 1985; Lyman et al. 2007; Shinoda et al. 2009), the latitudinal extent of the signals of 17-day TIWs is narrower, in which significant variability is found within 4°N and 4°S. The maximum of SSH fluctuation is found around 2–3°S, 120°W, and there is another local maximum in the northern hemisphere around 2°N, 120°W. The maximum in the northern hemisphere is smaller than but comparable to that in the southern hemisphere. This result is consistent with the analysis of TOGA TAO data along 140ºW, which indicates that the subsurface temperature (thus thermocline depth) signal associated with 17-day TIWs has maxima around 2°N and 2°S, and the one in south is larger (Lyman et al. 2007).

Figure 2b shows TIW activity calculated from the same analysis using the TMI SST. The maximum of SST fluctuations is found around 1°N, 120°W, which is closer to the equator than that for the SSH fluctuation. The maximum in the southern hemisphere is much smaller than that of the northern hemisphere. This is partly because the SST fluctuation in the northern hemisphere is primarily governed by the perturbation meridional velocity and the mean meridional temperature gradient. A previous observational study indicates that the perturbation meridional velocity associated with 17-day TIWs is maximum on the equator (Lyman et al. 2007), which is consistent with the characteristics of Yanai wave. The mean meridional temperature gradient is much larger in the northern hemisphere than in the southern hemisphere around this longitude. Hence, the maximum SST fluctuation associated with 17-day TIWs around 1°N is generated by a combination of the large meridional temperature gradient and strong TIW meridional velocity around this location. The location of the maximum is similar to that associated with 33-day TIWs in which the maximum is found around 2°N, 120°W (Shinoda et al. 2009). It should be noted that dominant processes that cause SST fluctuations associated with 17-day TIWs in the southern hemisphere is still uncertain without a full description of their velocity field.

Since the spectrum of SSH shows distinct spectral peaks for the first and second baroclinic modes of Yanai waves (Fig. 1a), it is plausible that SSH and SST signals around ~17 days and wave length ~1500 km shown in Fig. 2 are the mixture of these two modes. To separate the signals of 17-day TIWs into first and second baroclinic modes, SSH and SST time series are filtered in space and time for the area surrounded by the upper and lower boxes in Fig. 1b that cover the peak around the first and second baroclinic mode dispersion curves, respectively. Figure 3a shows the standard deviation of SSH time series at each location that

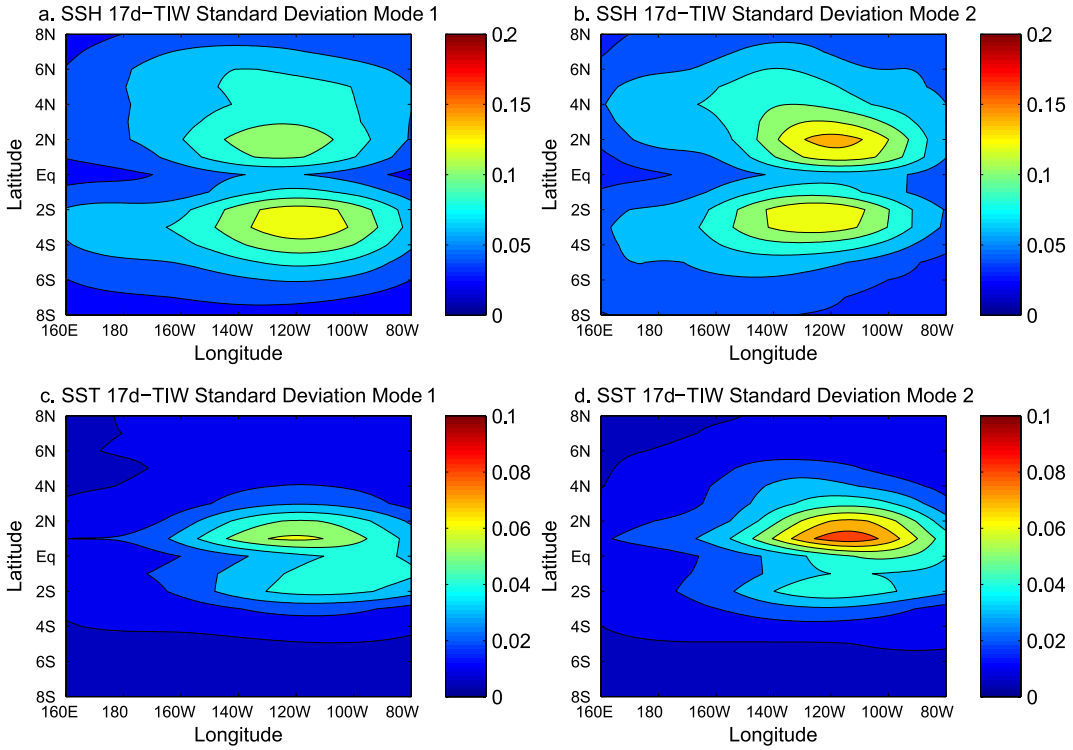

Fig. 3. (a) Same as Fig. 2a except time series are filtered at periods and wavelengths in the area surrounded by the upper box in Fig. 1b. (b) Same as Fig. 2a except time series are filtered in the area at periods and wavelengths in the area surrounded by the lower box in Fig. 1b. (c) Same as (a) except for SST anomalies. (d) Same as (b) except for SST anomalies.

are filtered for the area surrounded by the upper box. The spatial distribution of the SSH fluctuation around these wavenumbers and frequencies is similar to that for the total (first mode + second mode) variation. As in Fig. 2a, the maximum in the southern hemisphere is larger than that in the northern hemisphere for the first baroclinic mode.

Figure 3b shows the standard deviation of SSH time series for the second baroclinic mode which are filtered in space and time for the area indicated in the lower box in Fig. 1b. The spatial pattern of SSH fluctuation is notably different from that for the first baroclinic mode. While the distribution in the southern hemisphere is similar to that for the first mode, the maximum amplitude in the northern hemisphere around 2°N, 120°W is larger than that in the southern hemisphere. The spatial distribution in the northern hemisphere is similar to that in Fig. 2a, suggesting that a significant portion of 17-day TIWs variability in the northern hemisphere is associated with second baroclinic mode Yanai waves.

Figures 3c and 3d show the standard deviations of filtered SST time series at each location for the first baroclinic mode and the second baroclinic mode, respectively. The spatial pattern of the amplitude of first and second baroclinic modes are similar to that for the total (Fig. 2b), but the amplitude for the second baroclinic mode is larger than that for the first baroclinic mode. As shown in Figs. 3a and 3b, the amplitude of SSH fluctuation (and thus velocity) in the northern hemisphere is larger for the second baroclinic mode. Because of the large meridional temperature gradient in the northern hemisphere, the stronger meridional velocity for the second mode at this location causes large SST fluctuation.

Despite the limited resolution of the data, we found remarkable differences in spatial distribution of the amplitude of 17-day TIWs associated with first and second baroclinic mode Yanai waves. The spatial distributions for these modes in SST fields are consistent with those in SSH fields as shown in Fig. 3. Therefore we hypothesize here that the second baroclinic mode Yanai waves play a significant role in the SST and SSH variability caused by 17-day TIWs especially in the northern hemisphere.

3. Cross-correlation analysis

The phase relationships between SST and SSH associated with TIWs can be statistically described by a regression analysis (Shinoda et al. 2009). Time series of unfiltered SSH and SST anomalies are regressed against space and time filtered 17-day TIW SSH anomalies at 2.5°S, 123°W where the amplitude of 17-day TIW SSH fluctuation is maximum in Fig. 2a. Space and time filtered SSH anomalies used in the analysis include variability of both first and second baroclinic mode Yanai waves. Note that the data are not decomposed to symmetric and anti-symmetric components for the regression analysis.

The spatial pattern of these variables (Fig. 4) indicates that both SSH and SST variations associated with 17-day TIWs are nearly anti-symmetric with regard to the equator. However, the phase relationship between SST and SSH is different in northern and southern hemispheres. The maximum positive (negative) SSH anomalies in the southern hemisphere is located slightly west of the corresponding negative (positive) anomalies in the northern hemisphere. On the other hand, the maximum positive (negative) SST anomalies in the southern hemisphere is located slightly east of the corresponding negative (positive) anomalies in the northern hemisphere. As a result, the SST and SSH are nearly in phase in the southern hemisphere while the SSH and SST are nearly in quadrature in the northern hemisphere. The difference in phase relationship in northern and southern hemispheres could partly be attributed to the difference in mean currents that may impact on first and second baroclinic modes differently. The spatial pattern of SSH and SST anomalies for the first and second baroclinic modes show similar phase relationships to those shown in Fig. 4 (not shown).

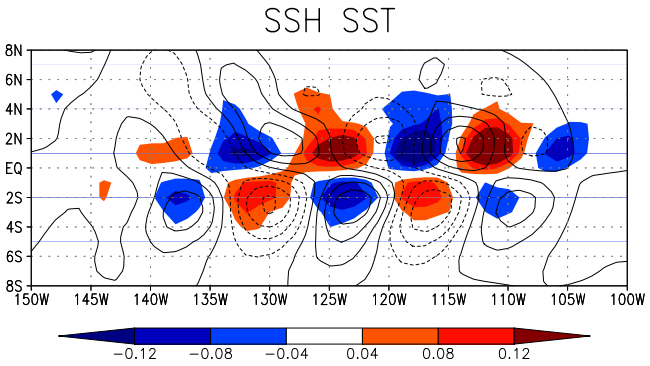

Fig. 4. SST (shading) and SSH (contour) anomalies regressed onto space and time filtered SSH anomalies at 2.5°S, 123°W. The contour interval is 0.05 cm. The solid (dashed) contour indicates positive (negative) values.

4. Conclusions

Because of the recent improvement of satellite-derived SSH fields, the observed dispersion relation of oceanic Yanai waves can now be described. Also, a zonal structure of 17-day TIWs, which have characteristics of Yanai waves, can be resolved by recent SSH products. Our results demonstrate that signals of oceanic Yanai waves can be isolated by wavenumber-frequency spectral analysis of high resolution SSH fields derived from recent satellite altimeter measurements. Also, salient features of 17-day TIWs such as the phase relationship between SSH and SST can be effectively isolated by a combination of wavenumber-frequency spectral analysis and regression. The statistical representation of these waves will be useful for evaluating ocean model performance in simulating 17-day TIWs, since models are not able to simulate individual TIWs. Also, the description of spatial pattern of 17-day TIWs is important for our understanding their dynamics.

Acknowledgments

The altimeter products were produced by Ssalto/Duacs and distributed by Aviso, with support from Cnes (http://www.aviso.oceanobs.com/duacs/). The TMI data are obtained from the Remote Sensing Systems web site. Valuable comments from George Kiladis are appreciated. Constructive comments from two reviewers are gratefully acknowledged. Toshiaki Shinoda is supported by NSF Grants OCE-0453046, ATM-0745897 and AGS-0966844, Office of Naval Research (ONR) Grant N0001410 WX20722, and the 6.1 project Global Remote Littoral Forcing via Deep Water Pathways sponsored by ONR under program element 601153N.

References

Chelton, D. B., and M. G. Schlax, 2003: The accuracies of smoothed sea surface height fields constructed from tandem altimeter datasets, *J. Atmos. Oceanic Technol.*, **20**, 1276–1302.

Cravatte, S., J. Picaut, and G. Eldin, 2003: Second and first baroclinic Kelvin modes in the equatorial Pacific at intraseasonal time scales. *J. Geophys. Res.*, **108**(C8), 3266, doi:10.1029/2002JC001511.

Farrar, J. T., 2008: Observations of the dispersion characteristics and meridional sea-level structure of equatorial waves in the Pacific Ocean. *J. Phys. Oceanogr.*, **38**, 1669–1689.

Halpern, D., R. A. Knox, and D. S. Luther, 1988: Observations of 20-day meridional current oscillations in the upper ocean along the Pacific equator. *J. Phys. Oceanogr.*, **18**, 1514–1534.

Itoh, H., and M. Ghil, 1988: The generation mechanism of mixed Rossby-gravity waves in the equatorial troposphere, *J. Atmos. Sci.*, **45**, 585–604.

Liebmann, B., and H. H. Hendon, 1990: Synoptic-scale disturbances near the equator. *J. Atmos. Sci.*, **47**, 1463–1479.

Lyman, J. M., G. C. Johnson, and W. S. Kessler, 2007: Distinct 17- and 33-day tropical instability waves in subsurface observations. *J. Phys. Oceanogr.*, **37**, 855–872.

Matsuno, T., 1966: Quasi-geostrophic motions in the equatorial area. *J. Meteor. Soc. Japan*, **44**, 25–43.

Miller, L., D. R. Watts, and M. Wimbush, 1985: Oscillations of dynamic topography in the eastern equatorial Pacific. *J. Phys. Oceanogr.*, **15**, 1759–1770.

Qiao, L., and R. H. Weisberg, 1995: Tropical instability wave kinematics: Observations from the Tropical Instability Wave Experiment (TIWE). *J. Geophys. Res.*, **100**, 8677–8693.

Shinoda, T., P. E. Roundy, and G. N. Kiladis, 2008: Variability of intraseasonal Kelvin waves in the equatorial Pacific Ocean. *J. Phys. Oceanogr.*, **38**, 921–944.

Shinoda, T., G. N. Kiladis, and P. E. Roundy, 2009: Statistical representation of equatorial waves and tropical instability waves in the Pacific Ocean. *Atmos. Res.*, **94**, 37–44.

Takayabu, Y. N., and T. Nitta, 1993: 35 day period disturbances coupled with convection over the tropical Pacific Ocean. *J. Meteor. Soc. Japan*, **71**, 221–246.

Wakata, Y., 2007: Frequency-wavenumber spectra of equatorial waves detected from satellite altimeter data. *J. Oceanogr.*, **63**, 483–490.

Weisberg, R. H., A. Horigan, and C. Colin, 1979: Equatorially trapped Rossby-gravity wave propagation in the Gulf of Guinea. *J. Mar. Res.*, **37**, 67–86.

Wheeler, M., and G. N. Kiladis, 1999: Convectively coupled equatorial waves: Analysis of clouds and temperature in the wavenumber-frequency domain. *J. Atmos. Sci.*, **56**, 374–399.

Wunsch, C., and A. E. Gill, 1976: Observations of equatorially trapped waves in Pacific sea level variations. *Deep-Sea Res.*, **23**, 371–390.

Yanai, M., and T. Maruyama, 1966: Stratospheric wave disturbances propagating over the equatorial Pacific. *J. Meteor. Soc. Japan*, **44**, 291–294.

Yanai, M., and Y. Hayashi, 1969: Large-scale equatorial waves penetrating from the upper troposphere into the lower stratosphere. *J. Meteor. Soc. Japan*, **47**, 167–182.

Zangvil, A., 1975: Temporal and spatial behavior of large-scale disturbances in tropical cloudiness deduced from satellite brightness data. *Mon. Wea. Rev.*, **103**, 904–920.

Zhu, X. H., A. Kaneko, N. Gohda, H. Inaba, K. Kutsuwada, and M. H. Radenac, 1998: Observation of mixed Rossby gravity waves in the western equatorial Pacific, *J. Oceanogr.*, **54**, 133–141.

Manuscript received 26 November 2009, accepted 25 January 2010
SOLA: http://www.jstage.jst.go.jp/browse/sola/